



Active and passive seismic data integration for delineating the near-surface velocity models at Ras Samadai area, Red Sea-Egypt

Ahmed Hamed¹ · Raafat Elshafie Fat-Helbary¹ · Ahmed M. Abdel Gowad²

Received: 16 May 2024 / Accepted: 2 June 2024 / Published online: 3 July 2024
© The Author(s), under exclusive licence to Springer Nature Switzerland AG 2024

Abstract

Shear-wave velocity is a soil mechanical property. It is the main cause of local ground-motion amplification, and it is responsible for a large amount of the damage. Therefore, it is crucial to investigate the soil characteristics down to bedrock to investigate the potential site effect. In this study, seven points in Ras Samadai area have been chosen to be investigated using Multichannel Analysis of Surface Waves (MASW) and Shallow Seismic Refraction (SSR) as active seismic methods. Furthermore, the Frequency-Wavenumber ($f-k$) and Horizontal-to-Vertical Spectral Ratio (HVSr) techniques were used as passive techniques to obtain the subsurface seismic velocity models and evaluate the site effect beneath the investigated points. The shallow and deep 1-D shear wave velocity models have been obtained at the chosen points using the MASW and $f-k$ approaches. Furthermore, the research area is divided into three main layers based on the seismic refraction approach. At certain cross-sections, there are clear variations in the layers thickness resulting from faults effect. The HVSr method displays two different kinds of curves: flat and one peak curves, due to the variation in impedance contrast between the bedrock and the overlying soil. Moreover, the obtained vulnerability index (K_g) indicates that there is low level of hazards could happen in the study area. Finally, the 2-D lithological models are created to delineate the underground fault lines and displays the lateral variations in lithological composition. This information is useful for the seismic hazard analysis in terms of ground response prediction at ground surface and soil column.

Keywords Shear wave velocity · Site effect · MASW · Frequency-Wavenumber array · Vulnerability index

Introduction

The area of Ras Samadai is situated along the shoreline of the Red Sea (Fig. 1). Whereas, the seafloor spreading is an essential characteristic of the Red Sea, along which the earthquakes activity indicates the spreading axis' location as well as the locations of the main transform faults (Bird et al. 2002; Augustin 2014; Mitchell and Augustin 2017). The Red Sea cities along the Egyptian coastal regions have witnessed some developments in the recent years due to increased population and tourism. These developments are probably going to continue in the

future. Accordingly, one of the main factors affect the new cities growth and expansion is the earthquakes activity around those cities and the geophysical characteristics of the construction soil (Gazetas 2006; Toni 2007). Hence, due to local ground-motion amplification (Idriss 1990), cities along the Red Sea coasts have suffered varying degrees of damage from historical and recent earthquakes (e.g. Hurghada city). Two significant events are listed in the Red Sea seismic activity catalogue, one of which had a magnitude of $m_b=6.1$ on November 12, 1954. This event's epicenter was close to the Abu Dabbab region. In addition, on July 2, 1984 another large earthquake of magnitude $m_b=5.1$ happened in the same active zone of Abu Dabbab. Additionally, other earthquake swarms (1976, 1984, 1993) were detected by the Egyptian national seismic stations at the same epicenters (Hamada 1968; Hassoup 1987; Kebeasy 1990; Azza et al. 2012).

In earthquake engineering, the shear-wave velocity (V_s) of the surface/subsurface soil layers is considered a significant parameter for its influence on local ground-motion amplification (Kagawa 1996; Li et al. 2016), which in turn is responsible for a great percentage of the damage in inhabited

✉ Ahmed Hamed
ahmadhamed4@nriag.sci.eg

Ahmed M. Abdel Gowad
ahmed.ghareb1@sci.svu.edu.eg

¹ National Research Institute of Astronomy and Geophysics,
Aswan 11421, EG, Egypt

² Geology Department, Faculty of Science, South Valley
University, Qena, Egypt

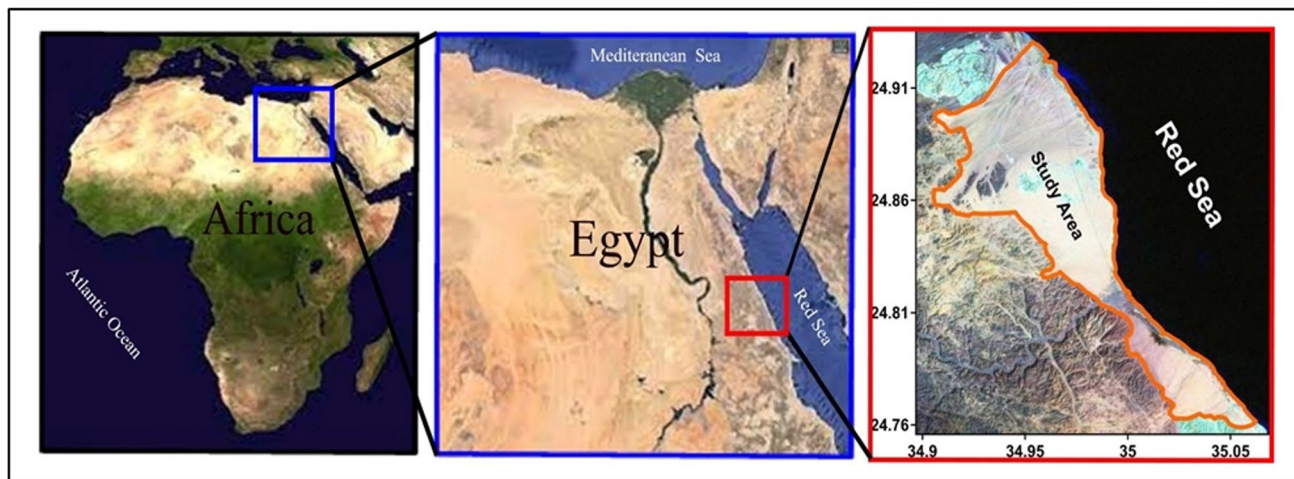


Fig. 1 Location map of the study area

regions (Bard 1994). Nondestructive methods are becoming more and more popular for measuring the variations in shear wave velocity across a soil for practical and economic reasons (Martínez-Soto et al. 2021; Kim and Hwang 2024). Thus, the underlying ground conditions might result in large amplifications because of the substantial impedance difference between a hard basement and soft soils.

In the current study, four seismic survey techniques have been applied (Mahajan et al. 2011; Nath et al. 2018), in order to construct 1-D V_s and 2-D V_p models. The commonly employed active techniques are the Multichannel Analysis of Surface Waves (MASW) and Shallow Seismic Refraction (SSR) (Mohammed et al. 2020). The analysis of surface wave dispersion is the basis of the MASW method (Park et al. 1999). However, the shallow seismic refraction approach makes it easier to characterize relatively large amounts of the subsoil by providing 2-dimensional cross-sections that include both distance and depth (Steeple 2005; Stipe 2015).

Furthermore, Boore et al. (1997) stated out that the decision to utilize the average shear-wave velocity extracted using the MASW approach down to a depth of 30 m as a variable to describe the site conditions, was made due to the comparatively limited availability of velocity data for further depths. Therefore, it is important to obtain a more detailed V_s profile. Because of this, the f - k array approach has been applied to accomplish this goal (Capon 1969; Ohori et al. 2002; Okada and Suto 2003). As a result, the combination of these techniques permits the extraction of numerical data on S-wave velocity models for the research area and for studying the medium's deeper characteristics. Furthermore, site effect is now an essential element for the evaluation of seismic hazards (Kramer 1996; Koller et al. 2004; Volant et al. 1998; El-Hussain et al. 2014). With the use of the dominant frequency (f_0), amplitude (A_0), and seismic vulnerability index (K_g), the soil

and the geological characteristics of the site could be evaluated to display how much damages of an earthquake cause. Hence, seven points have been chosen in the study area for applying the active and passive seismic techniques to identify the subsurface layers and assess the site effect (Fig. 2).

Local geology of the study area

The Miocene and younger sedimentary deposits are found in the research area. The Um Mahara Formation is observed as a series of moderate hills in the northwest

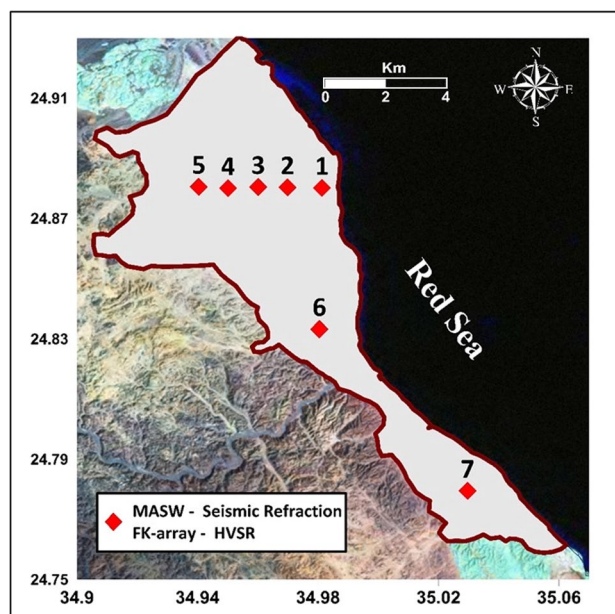


Fig. 2 Passive and active seismic wave measurement methods

close to the Wadi Ghadir entrance (middle portion of the research area). This formation consists of fossiliferous limestone with a gypsum top and sandy limestone at the bottom (Samuel and Saleeb-Roufaiel 1977). The evaporites and algal laminitis of the Ranga Formation lies beneath the Um Mahara Formation with a separation of small unconformity surface of a tiny layer of conglomerate. The second formation, called Um Gheig, is a thick dolomitic layer that sits above Abu Dabbab and is dispersed throughout the northern part of the present research area. The more calcareous Shagra Formation is located along the coast in the study area (Figs. 3 and 4). However, there is a connection between the sea level change and the current sabkha deposits. These deposits are loose sediments with a thickness ranging from 0.5 to 2 m, they include fine sands, silt combined with clay, intercalation with salts, anhydrite and gypsum lamina. Adjacent to the seashore, many phases of elevated beach sediments have been identified (Giegengack 1970 and Butzer and Hansen 1968). Coral reefs accumulate directly in front of the sea, and clastic beach sediments cover the reefs due to relative sea level variations acting as an indication of sea transgression. The upper portion of the raised beaches is made up of transported gravel coming from basement rocks, dolomite debris, shell fragments, and sand intercalations. The raised beaches are thought to be Pleistocene in age and could be categorized as coral reef rocks consisting of Reefal limestone with calcareous sandy, silt pockets, and old beach gravels. Furthermore, the present research area includes many locations where the recent Wadi deposits could be seen. Such deposits consist of loose rock fragments, gravels, sands with medium to coarse grains, and intercalation of varying volumes and thicknesses of gypsum and clay (Akkad and Dardir 1966a, b).

Methodology

The dispersion property of the surface waves forms the basis of the MASW and f - k Array methodologies (Park et al. 1999; Okada 2006). The V_s model may be derived by inverting surface-wave dispersion curves. Whereas, the surface waves are frequency dependent (Xia et al. 1999). Conversely, the shallow seismic refraction technique is a geophysical approach that has been used to produce two-dimensional profiles with depth and distance, which enable us to characterize comparatively vast regions of the subsurface by defining the underlying layers' velocity models. Moreover, the site effect has been studied by applying the HVSr approach to figure out the natural frequency, amplitude and vulnerability index (K_g) of the investigated points (Warnana et al. 2011; Molnar et al. 2018; Pamuk 2019).

Active seismic methods

Multichannel analysis of surface waves (MASW)

The Multichannel Channel Analysis of Surface Waves (MASW) method is the most widely used approach that uses Rayleigh wave analysis on a multi-channel record to obtain a shear wave velocity against depth (Park et al. 1998). The MASW technique's main benefits are that it takes much shorter time for collecting data from the field. Just one-shot gather is needed for a single source-receiver setup when using the MASW approach (Park et al. 1999). Whereas, the processing of all receiver data occurs simultaneously (Xia et al. 2002), and identification and elimination of noise sources is much easier (Park et al. 1999; Xia et al. 2002). As noise is reduced, the dispersion analysis becomes more accurate, which in turn produces a more accurate shear wave velocity model. During data collecting. Referring to Eq. (1) the longest surface wavelength is used to calculate the greatest depth of investigation (Z_{max}) (Park and Carnevale 2010).

$$Z_{max} \approx 0.5\lambda_{max} \quad (1)$$

The greatest depth of examination is correlated with the length of the receiver spread (L), which is also correlated with the longest wavelength that may be investigated (according to Eq. 2).

$$\lambda_{max} \approx L \quad (2)$$

Surface-wave (MASW) technique has been used in this work to provide a broad understanding of the subsurface geology (Craig and Hayashi 2016; Rehman et al. 2016; Salas-Romero et al. 2021); it might be integrated to provide important information for mitigating seismic risk. Currently, the main focus will be on active MASW surveys, producing a one-dimensional dispersion curve and therefore a one-dimensional shear wave velocity model.

Data acquisition and processing

Seven sites have been selected for this kind of measurement as part of the survey plan (Fig. 2), in order to get surface wave data. To acquire data, geophones with a frequency of 4.5 Hz are arranged in a straight line on the test site's surface and spaced apart by 2 m (geophone spacing). A data gathering instrument is attached to the geophones. Twenty-four geophones were chosen, and each is attached to a distinct recording channel (Park et al. 1997; Trupti et al. 2012; Foti et al. 2018; Aas and Sinha 2023; Meneisy et al. 2023). The sample interval is 1 ms sample (dt) and the entire total recording time (T) is typically about 1.5 s. A higher investigation depth is often the result of a stronger seismic source. A sledgehammer

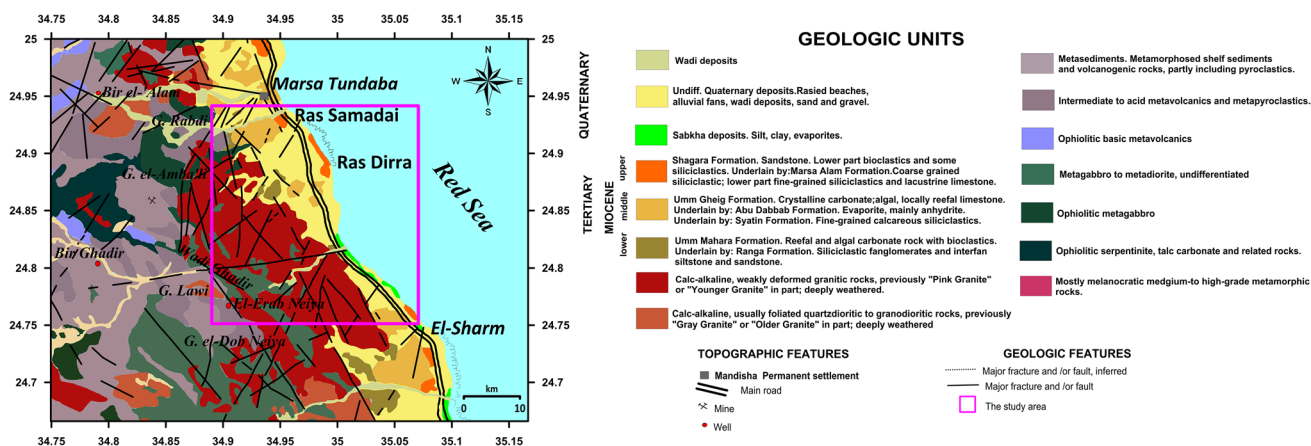


Fig. 3 Geology of the study area and its surroundings (after EGPC, Egyptian General Petroleum Corporation (EGPC), 1987)

that is fairly strong (e.g.10 kg) is a popular option. Using a metallic or non-metallic impact plate (base plate) may be useful in producing surface waves with a lower frequency. Practically, five strikes have been accumulated on the metal plate (Fig. 5). The offset (× 1) between the shot point and first geophone was selected to be 4 and 8 m, in order to improve the produced dispersion curve and enable observation of the near field and far field effects (Park et al. 2001).

Kansas Geological Survey (KGS 2006) developed the current used program of SurfSeis (V 4.0), in order to determine the shear-wave velocity model. Preprocessing was carried out to the data to allow to convert it from SEG-2 to KGS format to combine all of the separated shots into a single file (Fig. 6a). Field geometry is applied to the data based on the locations of the source and geophones as well as the distances between the receivers. Furthermore, it is possible to accept or reject the computed phase velocity-frequency curves based on the signal-to-noise ratio (Fig. 6b). The phase velocities-frequency dispersion curve of the fundamental mode is being carefully chosen between 5 and 105 Hz. The fundamental mode of the surface wave provides the required input data to perform the inversion. The fundamental mode curve is consistently becoming more common in the present study (Taipodia and Dey 2012).

The software's inversion procedure depends on the gradient iterative approach as outlined by Xia et al. (1999). The initial part of the inversion process involves evaluating a Vs profile whose theoretical dispersion curve matches the experimental one produced by the dispersion analysis. The shear wave's velocity is adjusted and updated with each iteration cycle. The Vs profile would be altered by the inversion if there is no matching, in which case the procedure would be repeated by calculating a new theoretical curve. These searching cycles, which continue until an appropriate match is found and a minimum root mean square error is reached, are properly referred

to as iterations (Park et al. 1999). The 1-D shear wave velocity model is obtained at the mid-point of the geophones line (Luo et al. 2009). Therefore, a 1-D velocity model will subsequently correspond to the soil components just beneath the center of a geophone spread (Figs. 6c and 7).

Shallow seismic refraction (SSR)

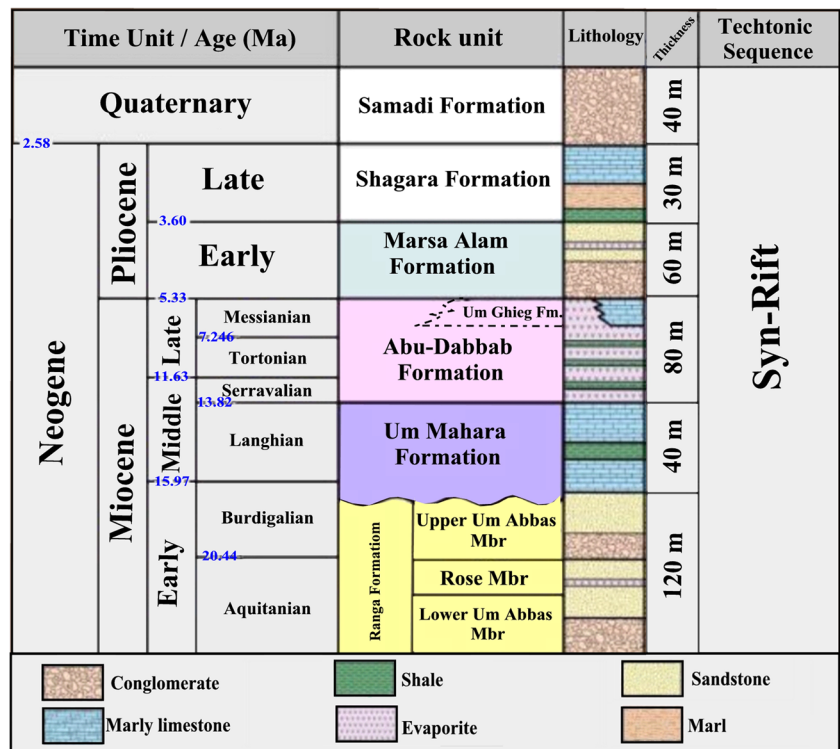
Seismic refraction tomography, also known as velocity gradient tomography, takes the seismic wave's initial arrival travel time as input (Zhu and McMechan 1989). Data processing and tomography interpretation are the next steps in the investigation after the collection of seismic refraction data. The term "P-wave" in engineering seismology is frequently used to refer to either the pressure wave, which is created by alternating compressions, or the main wave, which has the highest velocity and is hence the first to be collected (Báth 1978). Since P-wave always propagates longitudinally in isotropic and homogeneous materials, the solid's particle oscillations are parallel to or across the wave energy's travel direction. Equation (3) provides the velocity of P-waves in a homogeneous isotropic media.

$$V_p = \sqrt{\frac{K + \frac{4}{3}\mu}{\rho}} = \sqrt{\frac{\lambda + 2\mu}{\rho}} \tag{3}$$

where ρ is the density of the material the wave travels through, K is the bulk modulus, μ is the shear modulus, and λ is the first Lamé parameter. Conversely, density varies slightly, meaning that K and μ mostly determine the velocity. In Eq. (4), the elastic modulus P-wave modulus, M , is expressed as follows: $M = K + 4\mu/3$.

$$V_p = (M/P) \tag{4}$$

Fig. 4 Stratigraphic column of the study area (Modified after Khalil and McClay 2002)



Data acquisition and processing

To survey the research area, seven seismic refraction profiles were carried out using a seismograph equipped with 24 geophones (Fig. 2). Each profile is 115 m long overall. With

a total of 24 geophones per profile, the inter-geophone and shot to first geophone spacings were both 5 m. P-waves had a total recording length of 0.75 ms and a sampling interval of 0.25 ms. The seismic P-waves were produced using a sledgehammer reaching 10 kg. The P-waves are generated

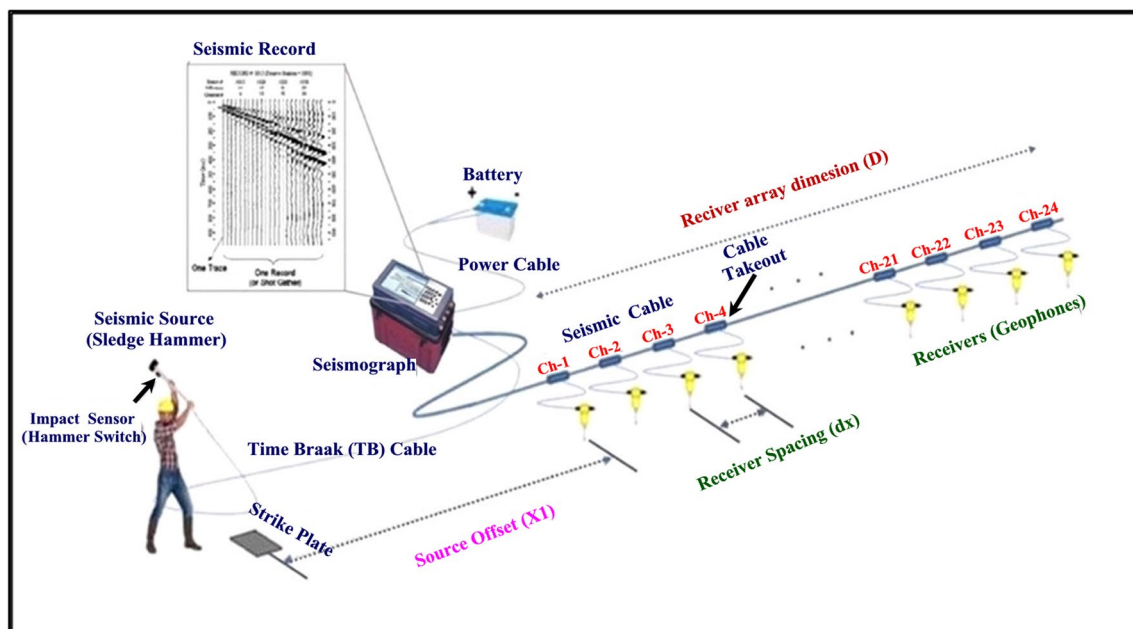


Fig. 5 Example of a MASW measurement profile. Lineup of 24 geophones with equal spacing (dx). The source offset is x_1

by striking a metallic plate ($20 \times 20 \text{ cm}^2$) with a sledgehammer. To reduce the noise level by as much as possible, three to five stacks were produced for every P-wave shot point (Klemperer 1987).

SeisImager software version 4.2 from Geometrics was used to determine the first arrival time (Fig. 8a). As shown in Fig. 8b, the travel time–distance curves have been generated using the selected timings as well as the distance from the receivers and the shooting locations (Báth 1978). After the velocity model produced by the time-term inversion, it is converted into an initial model, the tomographic inversion was carried out. This iterative process of tracing rays through the model aims to minimize the root mean square error (RMS) between the computed and observed travel-time curves (Schuster 1998). SeisImager performs the inversion using a least-squares method (Zhang and Toksoz 1998; Sheehan et al. 2005; Valenta and Dohnal 2007). It is clear that the underlying succession with the inverted velocities is represented by a three-layer cross-section (Figs. 8c and 9).

Passive seismic methods

Frequency—wavenumber (f - k)

The term "microtremors" describe very small vibrations with an amplitude of 10^{-2} to 10^{-4} mm that happen on the topmost layer of the earth (Mucciarelli et al. 2009). Its source is arbitrary and unidentified and they mostly travel in the form of wide-ranging, extremely dispersive surface waves travel throughout inhomogeneous rock and/or soil in the vicinity of the surface. Seismic investigation has made extensive use of these surface waves for studying the structure of the surface of the earth (Aki 1957; Ling 1994; Okada and Suto 2003; Okada 2006), enabling the study of the earth's deeper and shallower structure (Ling 1994; Shapiro and Campillo 2004; Okada 2006; Xu et al. 2012, 2013). Through an inversion technique, the dispersion characteristics of the surface waves may be utilized to determine Vs vs depth (Herrmann 1994 and Wathelet et al. 2004). The waves that affect vertical component are the Rayleigh-surface waves (Wathelet et al. 2004). This method needs collecting seismic noise simultaneously on several seismometers. There are several methods to obtain the dispersion nature of surface waves, in this work,

$$P(K_x, K_y, \omega) = \iiint_{-\infty}^{\infty} R(\xi, \eta, \tau) \exp\{i(\omega \tau - k_x \xi - k_y \eta)\} d\tau d\xi d\eta \quad (7)$$

where: $P(K_x, K_y, \omega)$ power spectral density function.

The phase velocity C_0 could be computed from the f - k spectrum peak that appears at coordinates k_{x0} and k_{y0} for a given frequency f_0 by Eq. (8):

we focus on the frequency–wavenumber (f - k) method (Aki 1957; Okada and Suto 2003; Wathelet et al. 2018).

Based on the assumption that plane waves travel throughout the array of sensors arranged at the surface, frequency–wavenumber (f - k) analysis calculates the relative arrival times at each sensor location and shifts the phases in accordance through the time delays. A wave with frequency (f), a direction of propagation, and a velocity (or equivalently, k_x and k_y , wavenumbers along x and y horizontal axis, respectively) is considered. All contributions will stack constructively if the waves move in a certain direction and at a certain speed, producing a high array output known as the beam power (Capon 1969). The azimuth and velocity of the traveling waves across the array may be estimated from the position of the maximum beam power in the plane (k_x, k_y). Microtremors are a phenomenon that depends on the position vector ξ (x, y) and the time t . A spectral representation is a record of microtremors over a defined period of time (Eq. 5).

$$x(x, \xi)(-\infty < t < \infty, -\infty < x < \infty, -\infty < y < \infty) \quad (5)$$

Assume that a microtremor sample function that has been acquired is a stationary stochastic process that is continuous with respect to t and ξ and has an average of 0. $Z^1(\omega, k)$ is a doubly orthogonal process, and $X(t, \xi)$ can be represented spectrally according to Eq. (6):

$$X(t, \xi) = \iiint_{-\infty}^{\infty} \exp(i\omega t + ik) dZ^1(\omega, k) \quad (6)$$

where $\omega = 2\pi f$ and $k = (k_x, k_y)$. In these expressions, ω is the angular frequency, k is the wavenumber vector, and k_x and k_y are its x and y components, respectively.

In order to determine the velocity for various frequency bands and short time periods, the phases of each signal are altered and focused at a specified frequency. This results in varying arrival durations at each sensor for a given velocity and plane wave propagation direction (k_x, k_y). A semblance value is produced by stacking the shifted signals in the frequency domain. Microtremors can be regarded as a temporally and spatially stochastic process with propagating waves. The following Eq. (7) can be used to approximate the f - k spectra of microtremors.

$$C_0 = \frac{2\pi f_0}{\sqrt{k_{x0}^2 + k_{y0}^2}} \quad (8)$$

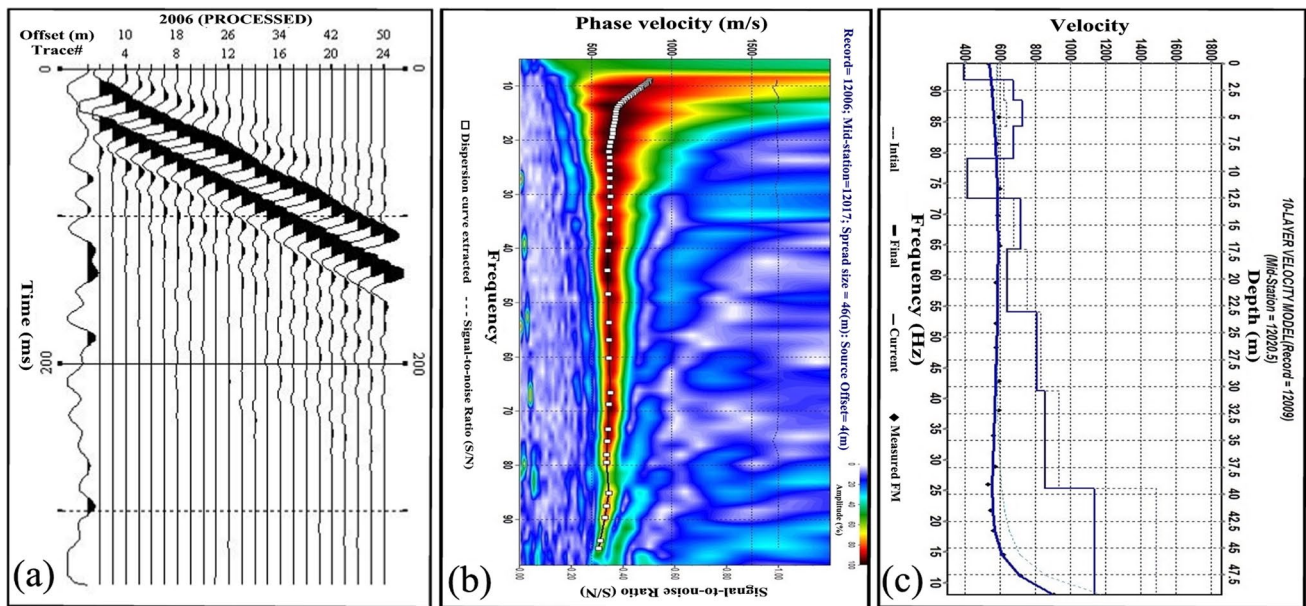


Fig. 6 Seismogram recorded from vertical impact sources at site 1 (a), the obtained dispersion curve (b), the inverted 1D-velocity model (c)

Data acquisition and processing

In the current research area, the ambient vibrations have been recorded at seven locations using an array of sensors. The measured sites' distribution is depicted in Figs. 2 and 10. Each array has a diameter of 100 m and four seismic stations arranged in a triangle or semi-circle shape with one station in the center and three of them at the vertices (Fig. 11a). At least 120 min for recording ambient noise simultaneously at all four stations are need for each array with 100 Hz sampling rate. The data was collected by portable seismic stations that were outfitted with a three-channel data logger model called Taurus (Nanometrics Co.). This data logger has a three-channel 24-bit digitizer and is coupled to a GPS receiver for position identification and time correction.

A flow chart for data processing utilizing the frequency-wavenumber approach is shown in Fig. 10. The vertical components are only impacted by the Rayleigh surface waves. Therefore, the processing of ambient vibration signals is limited to the vertical components (Fig. 11b) (Wathelet et al. 2004; Picozzi et al. 2005). Utilizing the frequency-wavenumber (*f-k*) approach, the back-azimuth and slowness of coherent seismic waves were analyzed in high resolution using the GEOPSY program (<http://www.geopsy.org>). Actually, obtaining the dispersion curve is the primary objective of the initial data processing step. Consequently, for each array, the theoretical array response takes into account the actual array geometry that was calculated. The signals originating from the NE-SW direction that coincide with the position of major seismic sources of the ambient vibration wave field (Figs. 12a and b). After the spectral curve of

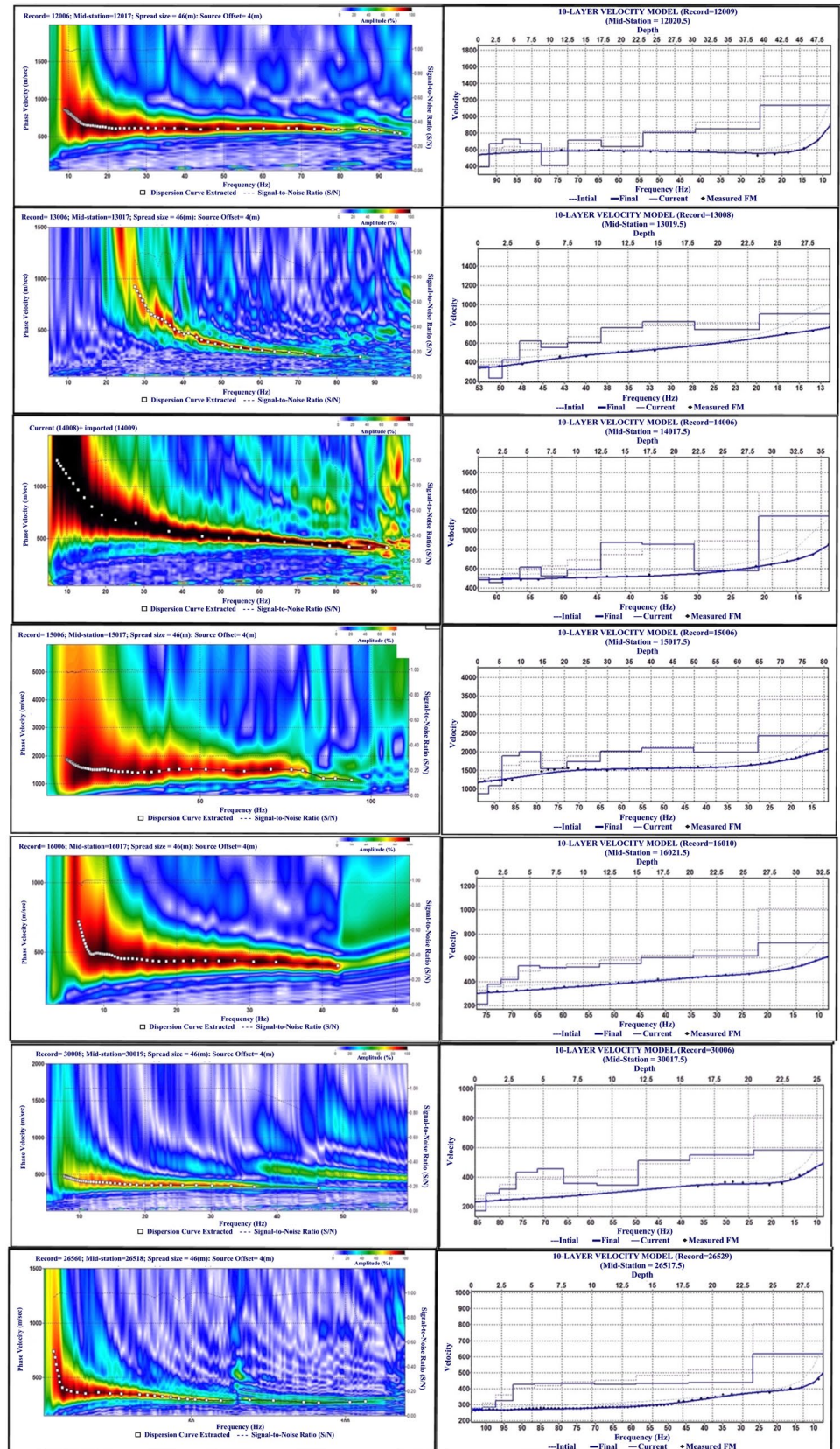
frequency range has been established, the dispersion curve has to be derived from the noise array signals. The waves that were captured split up into short periods of time. It varies in length depending on the frequency spectrum under consideration. Transients or saturated signals can be rejected using pre-processing techniques (Bard 1998 and Wathelet 2005).

Each sensor's signal undergoes a Fourier transform computation once the appropriate time windows are cut and a cosine taper is applied. Next, by utilizing the cut signals, the frequency-wavenumber transformation actually is computed in the frequency domain. The *f-k* approach yielded a dispersion curve with a black line and accompanying error bars at each frequency (Fig. 12c). Through the use of Dinver software, which implements the classical linearized algorithm, the resultant dispersion curves are finally obtained (Sambridge 1999a, b and Wathelet et al. 2018). Prior knowledge of many factors (such as the range of *V_p* and *V_s*, Poisson's ratio, and density) that may be obtained from seismic refraction and geological data about the area can be included through the inversion step, to show finally the 1-D *V_s* and eventually *V_p* profiles at the studied points (Fig. 13).

Horizontal to vertical spectral ratio (HVSr)

Nakamura (1989, 1996, 2000a, b) developed the H/V method, and he showed that the amplification factor corresponds to the fundamental frequency of the soil below the site, and in turn, related also to the ratio of the Fourier

Fig. 7 The obtained dispersion curves (a), the inverted 1-D shear wave velocity model at the selected site (b)



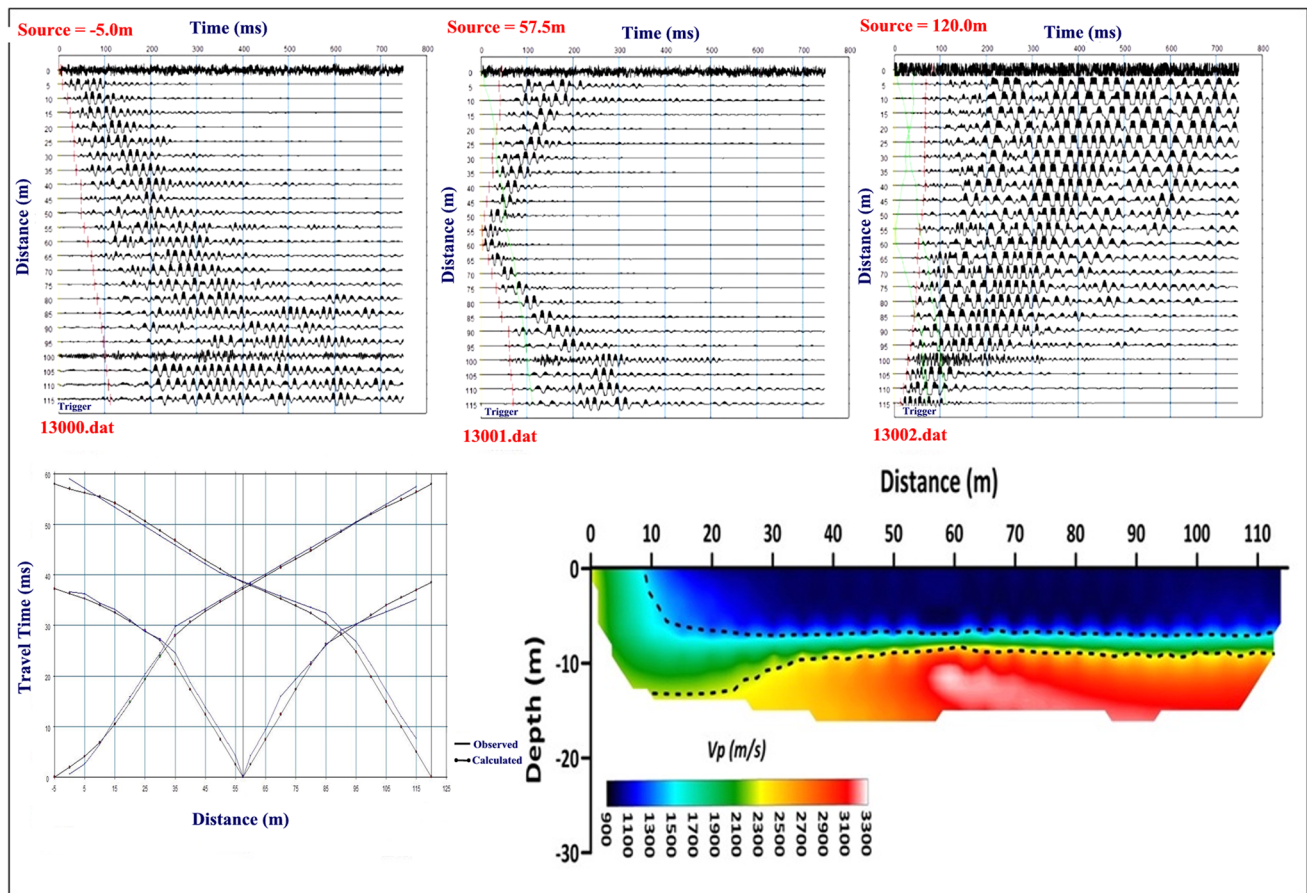


Fig. 8 Seismograms recorded from vertical impact sources at site 3, red bars represent picking of the first arrivals (a), the travel time-distance curve (b), the 2-D velocity model deduced from P-wave profile (c)

spectral amplitude of the horizontal to vertical component of the background noise records (microtremors) (D’Amico et al. 2008). The "surface waves" theory, which links HVSR to the frequency-dependent ellipticity of Rayleigh waves, is more often accepted (Bard 1998; Bonnefoy-Claudet et al. 2006). Numerous studies have demonstrated that if the higher layers have a strong impedance difference with the bottom stiffer layers, the ambient noise H/V spectral ratio is extremely concentrated around the basic S-wave frequency (Guillier et al. 2007; Mundepi and Kamal 2006). At every frequency, the HVSR values are described according to Eq. (9):

$$HVSR(f) = \frac{\sqrt{H_{NS}(f) \cdot H_{EW}(f)}}{V(f)} \tag{9}$$

where the horizontal and vertical component spectra are represented by the letters H and V. Equation (9) was used to derive the resulting horizontal component for the two horizontal ones, $H_{NS}(f)$ and $H_{EW}(f)$, and divide it by the vertical component $V(f)$ to determine the site's response.

Thus, for each (n) windows, the distribution of $\log_{10}(H/V)$ was obtained as a function of frequency. The average of H/V (H/V_{avg}) overall selected windows (n) was obtained using Eq. (10).

$$H/V_{avg} = \frac{\log_{10}(H/V)}{n_{windows}} \tag{10}$$

Whatever the case, the low frequency peak that surpasses two units of amplitude at each location was identified as the fundamental frequency (f_0) (SESAME 2004).

This study was carried out in an area where the Abu Dabbab active zone triggered earthquakes. The main target is to identify the features of soil deposits. Depending on the values of the amplification (A_0), dominant frequency (f_0) and seismic vulnerability index (K_g). The kind of soil and geological factors can influence how much destruction a seismic event cause. In order to expedite and correctly map regions susceptible to disasters and carry out mitigation actions. Hence, this approach is thought to be less expensive and simpler to execute. This may reduce the effect of earthquake-related destruction and fatalities.

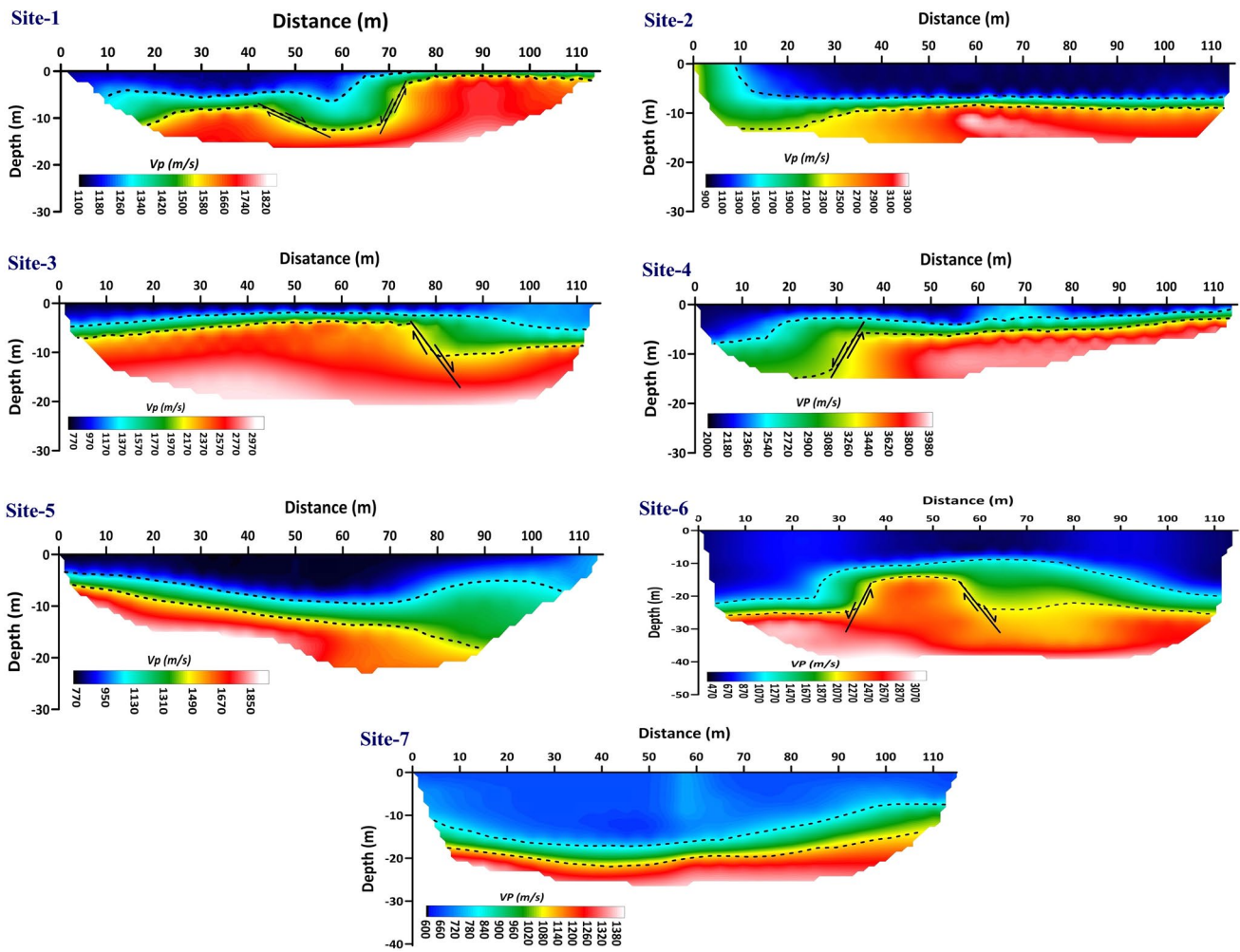
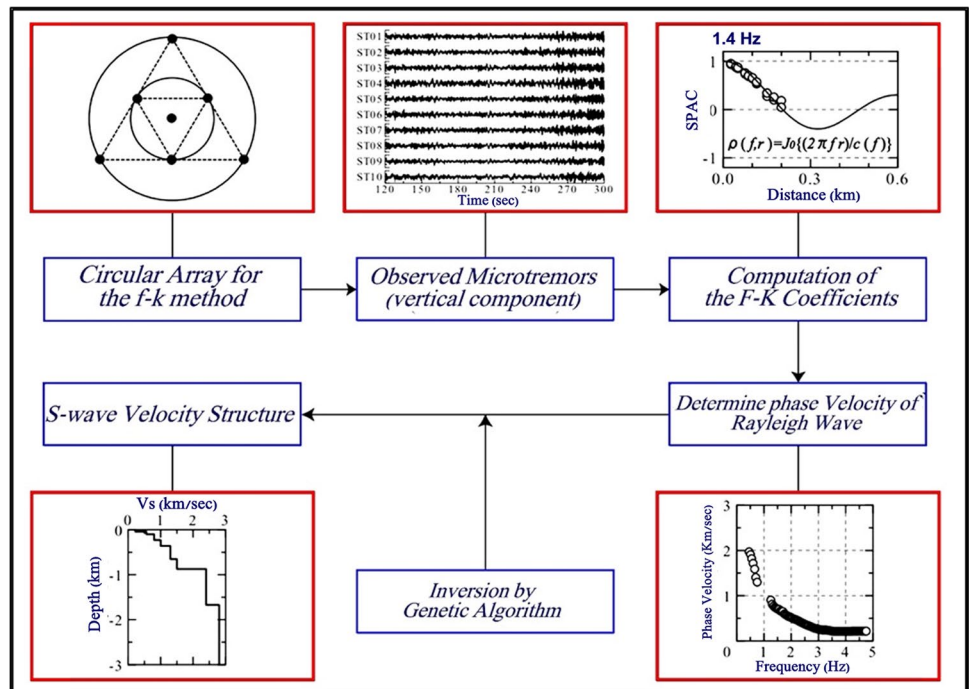


Fig. 9 The obtained 2-D velocity models deduced from seismic refraction method

Fig. 10 Flowchart of observation and analysis of the f - k method for estimating S -wave velocity structures using array observations of microtremors (Okada and Suto 2003)



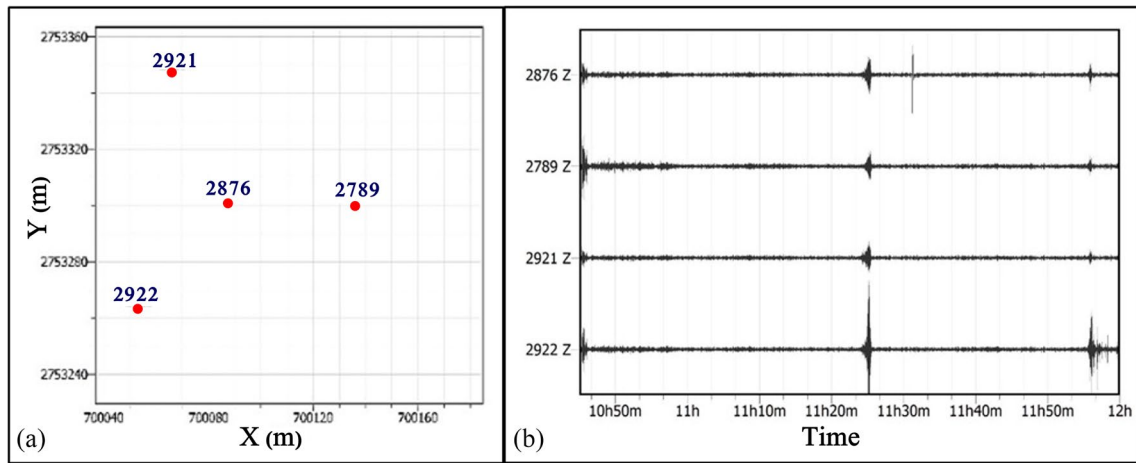
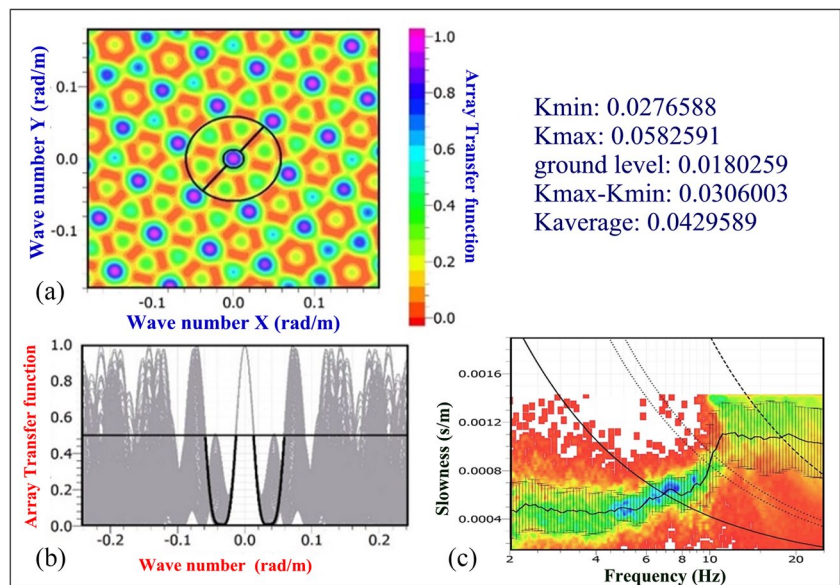


Fig. 11 Geometry of an array at site No.1, the distance between the sensor in the center and each sensor on the periphery is 100 m (a), example of ambient noise recorded by sensors array (b)

Fig. 12 Theoretical frequency-wavenumber response for site No.1 corresponding to array geometry (a), section across theoretical array response for various propagation azimuths (b), slowness histograms show the dispersion curve derived from *f-k* method (c)



Data acquisition and processing

The fundamental frequency in the present study is measured using the HVSR technique at seven points in Ras Samadai area, with a continuous ambient noise data collection period of around 120 min. The data set was gathered using Trillium compact 120 s sensor at a sampling rate of 100 Hz. For providing dependable experimental conditions, the recommendations put out by Koller et al. (2004) have been followed. We made all efforts to stay away from busy highways and subterranean buildings. The European project SESAME (2004) created the GEOPSY program which has been used in this study for the analysis of microtremor data. At least 10 non-overlapping windows have to be chosen, with time window value about 25 s and located in the quietest region of the

acquired signal (Fig. 14a). Based on a traditional comparison of the long-term average (LTA) and the short-term average (STA), windows are chosen. On each component, the Fast Fourier Transform (*FFT*) is used throughout the frequency computation procedure (Konno and Ohmachi 1998). Therefore, the related signal with a certain frequency is represented by its amplitude (Fig. 14b). Prior to dividing by the vertical component spectrum, the spectra of the two horizontal components were combined employing the geometric mean(Fig. 14c). Standard deviations can be determined at each frequency of interest by averaging the generated H/V's spectra. The next step would be to identify the fundamental resonance frequency at every point (Matsushima et al. 2014).

Every peak underwent reliability evaluation as well as an industrial or natural origin analysis (Fig. 14d). In order to

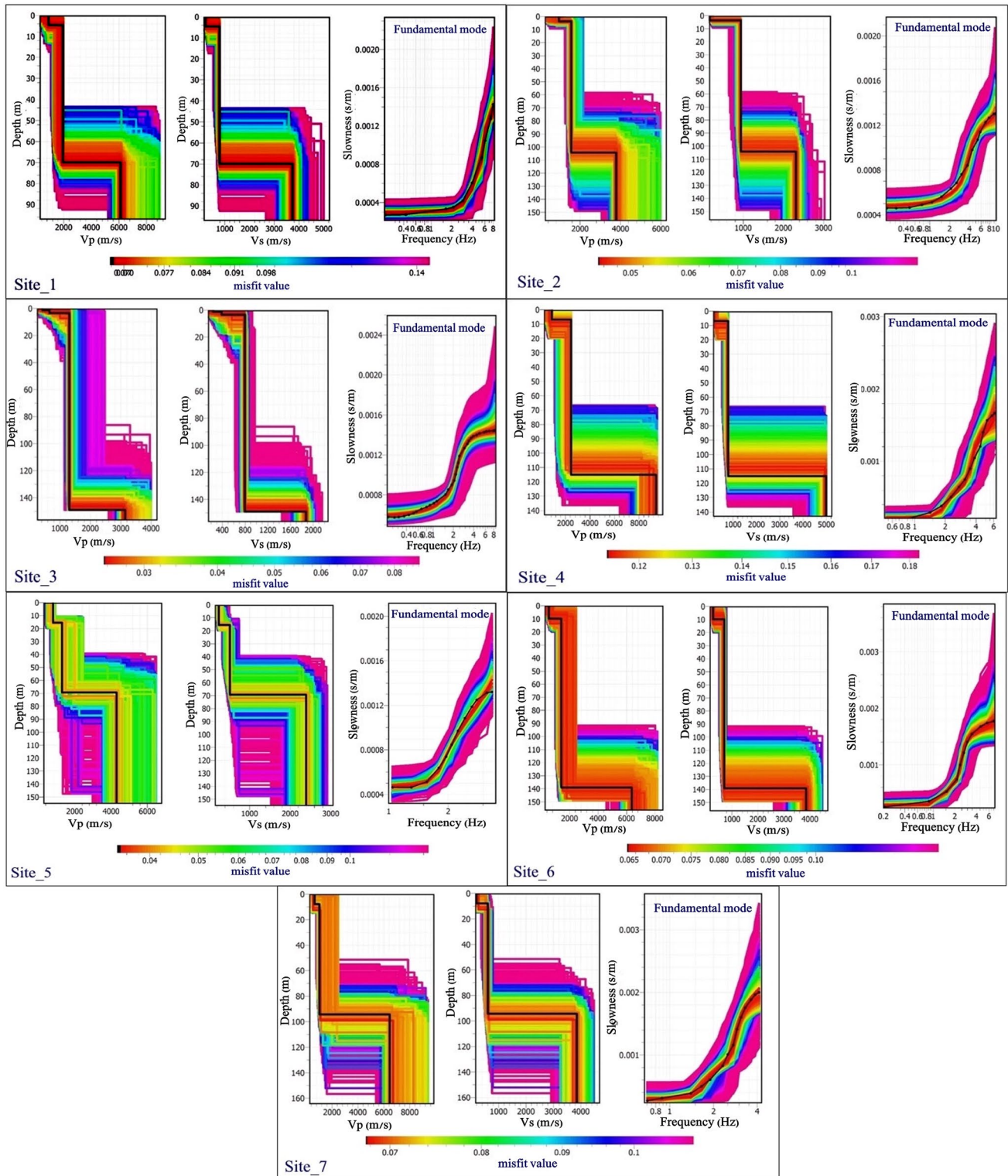


Fig. 13 The resulted 1-D velocity models obtained from the f - k analysis at the seven experimented sites. The inverted velocity models of V_p (left), V_s (middle) and dispersion curve (right)

have a distinct peak that is associated with several attributes, the trustworthy H/V curves need to meet stability requirements. H/V curves that failed to satisfy the majority of the

stability requirements for clear peaks and the key criterion for clear curves as stated by SESAME (2004) were deleted. In the current study, it was determined that the peaks that

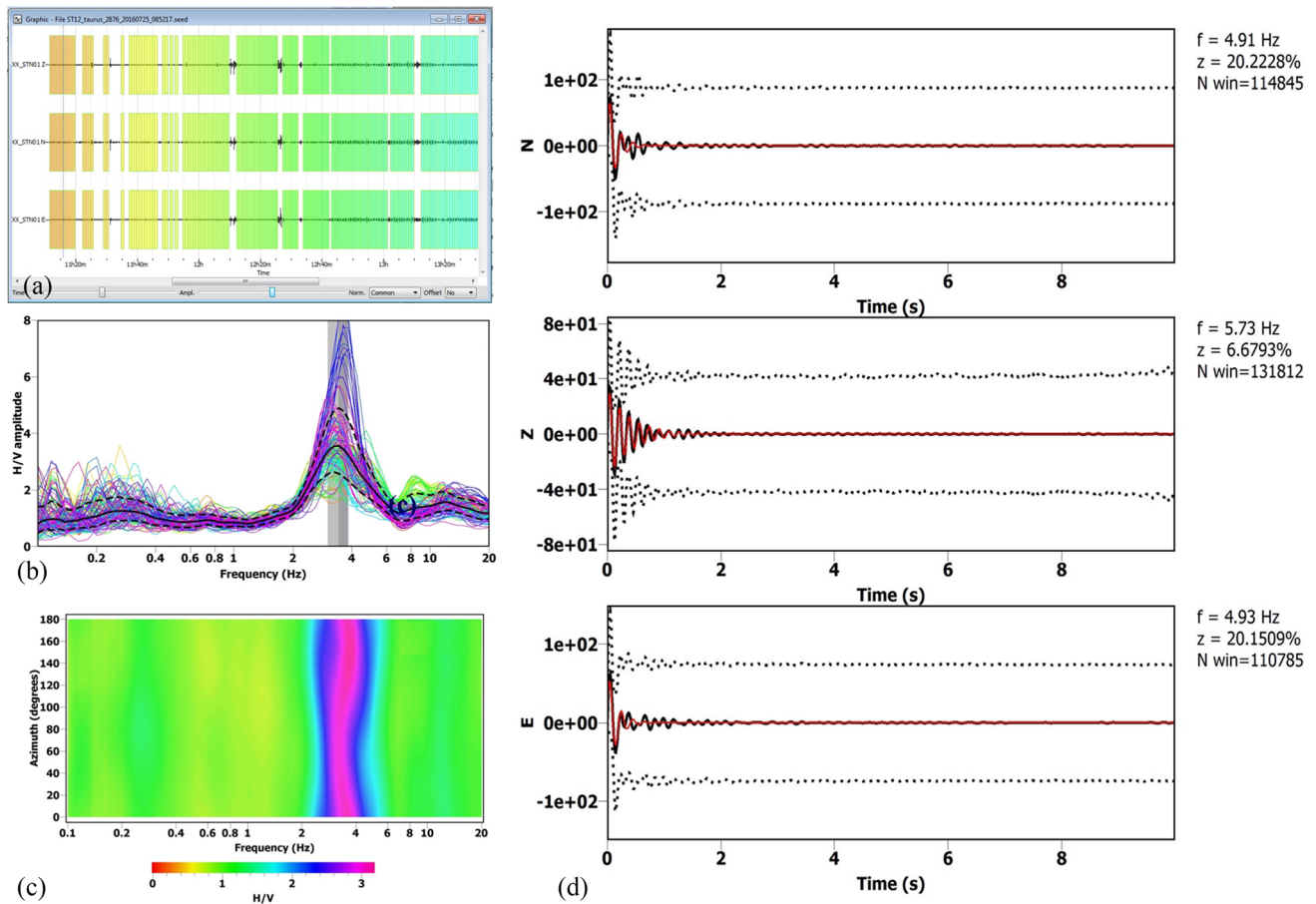


Fig. 14 The steps of HVSR processing. Windows selection for the recorded microtremor data (a), the H/V spectral ratio curve (b), the H/V rotation with azimuth degrees (c), the damping test for the peak amplitude at frequency 4.9 Hz which is of natural origin (d)

were obtained in the seven tested sites have natural origin (Fig. 15).

$$K_g = \frac{A_0^2}{f_0} \tag{11}$$

Estimation of the seismic vulnerability index (K_g)

The degree of susceptibility of the top soil layer to deformation during an earthquake is indicated by the seismic vulnerability index (K_g). The dominant period of the soil and the degree of the soil amplification factor have an impact on the seismic susceptibility index (Huang and Tseng 2002; Akkaya 2020; Rohmah et al. 2023). The susceptibility of any area to ground movement is assessed using the seismic vulnerability index (K_g). According to research conducted by Nakamura (2008), the value of the seismic vulnerability index indicates how much damage an earthquake could cause. Equation (11) calculates the seismic vulnerability index (K_g) by comparing the square of the amplification value (A_0) with the dominant frequency (f_0) in the research area (Nakamura 2000a, b).

Results and discussion

We have presented integrated seismic techniques in the current study, in order to delineate the subsurface velocity models and the site effect beneath seven selected points at Ras Samadai area along the Red Sea shoreline in Egypt. For data surveys, we used four seismic methods, MASW and shallow seismic refraction for 1-D and 2-D configurations respectively, for active experiments. While, in the passive experiment the f - k array and HVSR techniques applied for determining the deeper 1-D shear wave velocity models and site effect respectively. According to the 1-D shear wave velocity (V_s) models obtained from MASW

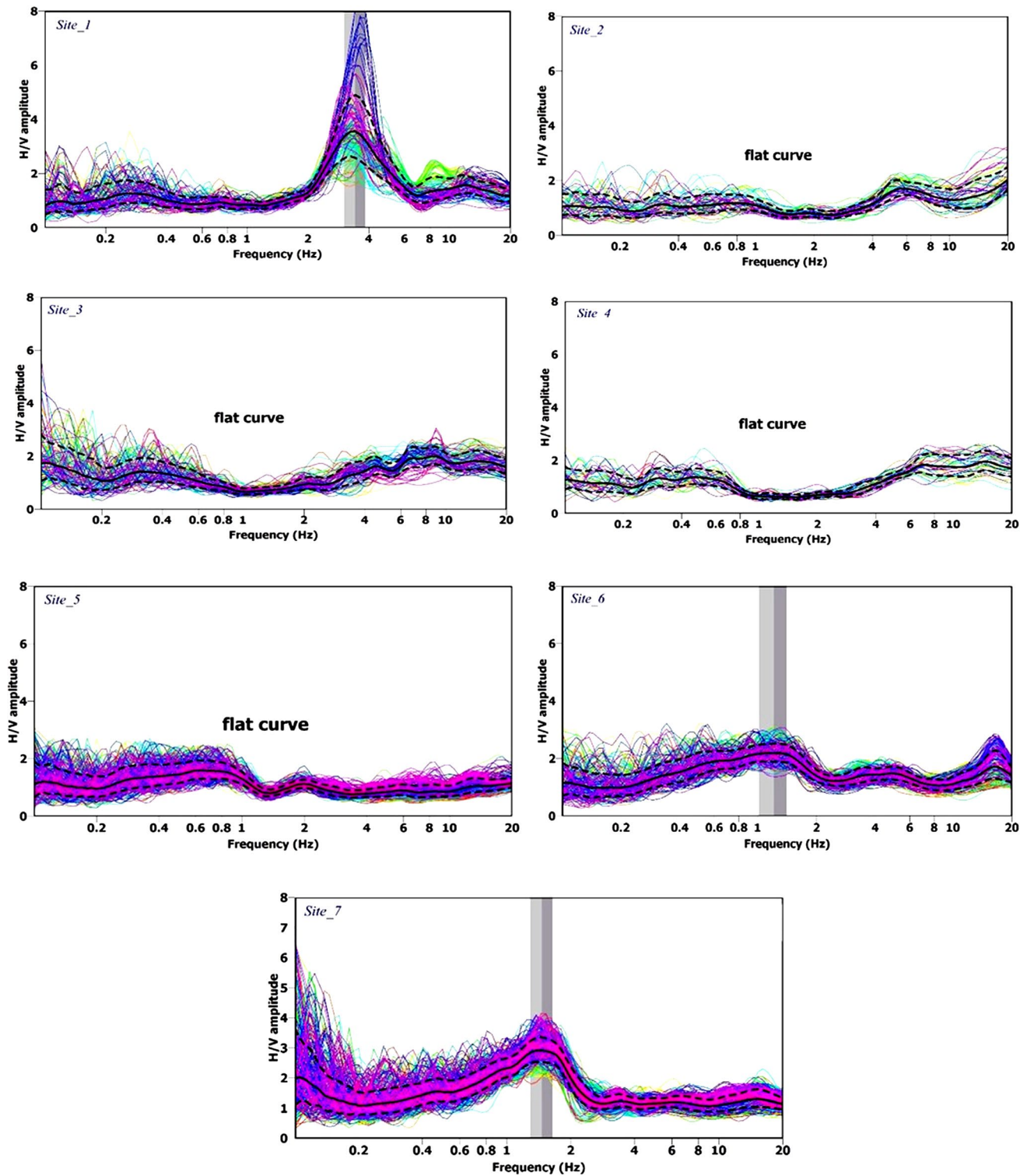


Fig. 15 The obtained HVSR¹ curves at the 7 selected sites in the study area

approach (Fig. 7). The uppermost layer in the area under investigation is thin and has low compactness. While, the deeper strata have higher shear wave velocities values (average 1800 m/s), which are indicative of highly compacted sandstone and

calcareous sandstone. However, it has been noted that, sites 6 and 7 have modest shear wave velocity values (less than 600 m/s) as a result of the dominance of substantial layers of loose Quaternary deposits at those locations.

Table 1 Calculated fundamental frequency, amplitude and vulnerability index for the selected study points

Site Code	Lat	Long	F_0	A_0	Kg
1	24.8796	34.9804	3.7	3.6	3.5
2	24.87867	34.96915	-	-	-
3	24.8801	34.95932	-	-	-
4	24.8801	34.94994	-	-	-
5	24.8796	34.93917	-	-	-
6	24.83199	34.98045	1.2	2.1	3.6
7	24.7794	35.03008	1.7	3.2	6.0

Table 2 Typical ranges of shear wave velocities for various types of soils (Telford & Sheriff 1984)

Soil type	Shear wave velocity (m/s)
Dry silt, sand, loose gravel, loam, loose rock, moist fine-grained top soil	180–750
Compact till, gravel below water table, compact clayed gravel, cemented sand, sandy clay	750–2250
Weathered rock, partly decomposed rock, fractured rock	600–3000
shale	750–3300
sandstone	1500–4200
limestone and chalk	1800–6000
igneous rock (granite, diabase)	3600–6000
metamorphic	3000–4800

Through the use of seismic refraction tomography, detailed information on the bedrock structure, velocity distribution, and depth of underlying strata have been obtained (Jakosky 1940). In the current study, the obtained 2-D cross-sections exhibit a general classification of the research area into three primary strata (Fig. 9). The top layer is mostly composed of loss sediments which characterized by low seismic wave velocity values (450–1100 m/s) and 7 m thickness. However, the thickness of this bed reaches up to 13 to 21 m at site 6 and 7. On the other hands, the second layer is defined by highly compacted calcareous sandstone, clay, and sandstone, with seismic velocity between 1100 to 2900 m/s. The third layer is composed of evaporates and calcareous sandstone, defined by high velocities values reach to 3900 m/s. The previous geological, structural and geophysical studies indicate that the variations in the layers thickness could be related to the presence of subsurface faults affecting the layers, as shown in Fig. 9.

On the other hands, the frequency-wavenumber (f - k) ambient vibration array method, is the first passive seismic technique used in the current investigation. These seismic wave measurements depend on how surface waves in stratified medium disperse. The ambient vibration (f - k) approach employs the microtremor data, and the dispersion curves

inverted into 1-D shear wave velocity models. When the inverted dispersion curve is compared to the observed one, a satisfactory match is obtained for all arrays. Figure 13 displays the 1-D V_p and V_s models together with the dispersion curves for each array with a colored scale representing the misfit amount. The phase velocity derived from the f - k analysis is indicated by the black line on the dispersion curve's fundamental mode. The black line linked to the smallest misfit represents the related average shear wave velocity structure of the inversion outcomes. The obtained models at the seven selected sites show that the values range from 3100 to 8100 m/s. The loss Quaternary deposits in this area are typically represented by the first layer, which has an average thickness of 7 m and a shear wave velocity of approximately 400 m/s. The second layer characterized by thickness variation, and could be considered as graben faults covering the first five tested points in the study area, it has average shear wave velocity value about 800 m/s and depths of around 70, 100, 140, 100, and 70 m from site 1 to site 5, respectively. Conversely, the velocity values at sites 6 and 7 range from 2200 to 4700 m/s due the existence of the basement rocks.

The HVSR technique, plays a significant role in the disaster mitigation by reducing the impact of casualties and damage. The current investigation shows HVSR peaks with a fundamental frequency ranging from 1.25 to 3.75 Hz (Fig. 15 and Table 1). Due to the velocity variation between the soil and the underlying bedrock, we had been obtained two different forms of curve topology, including a curve with one peak (clear peak) and a non-peak curve (flat curve). As seen in Fig. 15, the sites 1 and 7 have a single and distinct peak, indicates the presence of impedance contact at a specific depth. On the other hands, site 6 displays a broad peak curve, due to the occurrence of sloping basins or differences in the sedimentary structures of the bedrock. Conversely, at the other sites, the presence of compacted and stiff clay and sandstone on the surface do not exhibit any appreciable amplification and produces flat HVSR curves without any clear peak.

Additionally, the vulnerability index (Kg) employs the obtained data from HVSR technique to determine the places where a degree of seismic hazards and damage may be predicted. Referring to Table 1, the seismic vulnerability index (Kg) value varies from 3.5 to 6.0. The areas which characterize by low amplification (A_0) and high dominant frequency (f_0) values are said to have low seismic vulnerability index (Kg). On the other hand, the investigated points characterized by flat HVSR curves show no indication of liquefaction or vulnerability index.

The compilation and integration of the obtained 1-D shear wave velocity models from MASW and f - k arrays, and based on the standard values of the shear wave velocity for different rock types (Table 2), we succeeded to generate

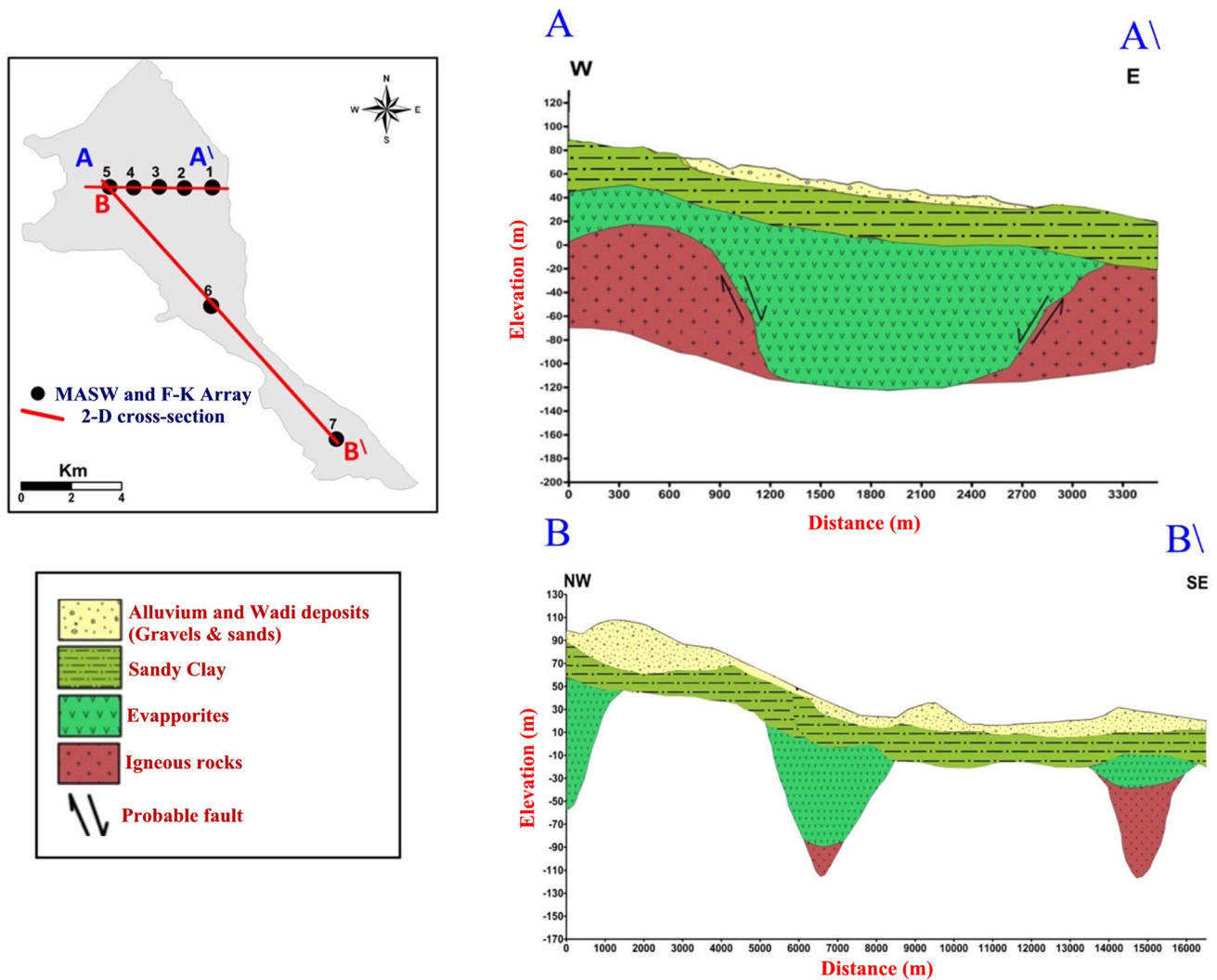


Fig. 16 The obtained 2-D- subsurface models according to the integrated velocities data

couple of 2-D lithological models pass through the investigated points. The cross-section presents the observed ground surface and underground fault lines and displays the lateral variation in lithological composition as seen in cross-section A-A' (Fig. 16). Consequently, from this study, the comprehensive soil information from the 2-D cross-sections is useful for the seismic hazard analysis in terms of ground response prediction at ground surface and soil column.

Conclusion

Seven locations in the Ras Samadai area, south of the Red Sea, have been selected for the studying, by implementing active seismic techniques, including Multichannel Analysis of Surface Waves and Shallow Seismic Refraction. Additionally,

Frequency-Wavenumber ($f-k$) array and the Horizontal-to-Vertical Spectral Ratio techniques were employed as passive methods to determine the subsurface seismic wave velocity models and to assess the site effect underneath the tested points. The shallow and deep 1-D shear wave velocity models have been obtained at the chosen points using the MASW and $f-k$ approaches respectively. Furthermore, the applied seismic refraction approach reveals that the surface/subsurface lithological succession of the research area is divided into three main layers. It has been discovered that the fault effect causes distinct differences in the thickness of the layers at certain cross-sections.

Due to the variation in the impedance contrast depth between the bedrock and the overlaying soil, the HVSR technique exposes two different kinds of curves: flat and one peak curves. Additionally, the vulnerability index (K_g) values show that the research area has a low degree of potential seismic

hazard. Furthermore, two-dimensional (2-D) lithological models have been developed from the 1-D shear wave velocity models to define the subterranean fault lines and illustrate the lateral variation in lithological composition. Finally, we could say this data is useful for seismic hazard assessments in terms of calculating ground response at the soil column and ground surface.

Recommendation

Because of the financial support's limitations, we can only say that the data set offers a comprehensive view of the subsurface structure in the research area. Therefore, an efficient investigation is needed to track any possible changes in the properties of the soil.

Acknowledgements We would like to thank the National Research Institute of Astronomy and Geophysics (NRIAG) and Aswan Regional Earthquake Research Center for providing us the equipment needed to do this research.

Author Contributions The study was conceptualized and designed with participation from all authors. The information compilation and data collection were under supervision of Ahmed Hamed. Ahmed Hamed and Ahmed M. Abdel Gowad, however, were in charge of the data analysis. Raafat El-Shafie Fat-Helbary and Ahmed Hamed wrote the paper's first draft, although all authors contributed feedback on earlier drafts and reviewed and approved the final manuscript.

Funding Not applicable.

Financial interests

The authors declare they have no financial interests.

Data availability Data are available from the authors upon reasonable request.

Declarations

Conflict of interest The authors declare that they have no conflict of interests.

References

- Aas A, Sinha SK (2023) Seismic site characterization using MASW and correlation study between shear wave velocity and SPT N. *J Appl Geophys* 215:105131. <https://doi.org/10.1016/j.jappgeo.2023.105131>
- Aki K (1957) Space and Time Spectra of Stationary Stochastic Waves, with Special Reference to Microtremors. *Bull Earthquake Res Institute* 35:415–459
- Akkad S, Dardir A (1966a) Geology of the Red Sea coast between Ras Shagra and Marsa Alam with short notes on results of exploratory work at Gabal EI Rusas lead-zinc deposits. *Geo! Surv. Egypt* 35, 67. Cairo
- Akkad S, Dardir A (1966b) Geology and Phosphate deposits of Wasif, Safaga area. In: 15 *Geol Surv and Min Res Dep Cairo*, paper no. 36, pp. 1–35
- Akkaya I (2020) Availability of seismic vulnerability index (Kg) in the assessment of building damage in Van, Eastern Turkey. *Earthq Eng & Eng Vib* 20(19):189–204. <https://doi.org/10.1007/s11803-020-0556-z>
- Augustin N, Devey CW, van der Zwan FM, Feldens P, Tominaga M, Bantan RA, Kwasnitschka T (2014) The rifting to spreading transition in the Red Sea. *Earth Planet Sci Lett* 395:217–230. <https://doi.org/10.1016/j.epsl.2014.03.047>
- Azza M, Hosny A, Gharib A (2012) Rupture process of shallow earthquakes of Abou-Dabbab area, south east of Egypt. *Egypt J Appl Geophys* 11(1):85–100
- Bard PY (1994) Effects of surface geology on ground motion: recent results and remaining issues. In: *Proc. of the 10th European Conf. on Earthquake Engineering*, Vienna, pp. 305–323
- Bard PY (1998) Microtremor measurements: A tool for site effect estimation? In Okada & Sasatani (eds) Irikura, Kudo, editor, *Proc. 2nd Intl. Symp. on The Effects of Surface Geology on Seismic Motion*, pages 1251–1279. Balkema, 1998
- Båth M (1978) An analysis of the time term method in refraction seismology. *Tectono-Physics* 51(3–4):155–169. [https://doi.org/10.1016/0040-1951\(78\)90238-X](https://doi.org/10.1016/0040-1951(78)90238-X)
- Bird P, Kagan YY, Jackson DD, Stein S, Freymueller JT (2002) Plate tectonics and earthquake potential of spreading ridges and oceanic transform faults. In *Plate Boundary Zones* (eds. Stein, S. & Freymueller, S. T.). <https://doi.org/10.1029/GD030p0203> (AGU, 2002)
- Bonnefoy-Claudet S, Cornou C, Bard P-Y, Cotton F, Moczo P, Kristek J, Fah D (2006) H/V ratio: a tool for site evaluation. Results from 1-D noise simulations. *Geophys J Int* 167:827–837
- Boore DM, Joyner WB, Fumal TE (1997) Equations for estimating horizontal response spectra and peak acceleration from western North American earthquakes: A summary of recent work. *Seismol Res Lett* 68:128–153
- Butzer KW, Hansen CL (1968) *Desert and river in Nubia*. Univ. Wisconsin Press, Madison, p 562
- Capon J (1969) High-resolution frequency-wavenumber spectrum analysis. *Proc IEEE* 57(8):1408–1418. <https://doi.org/10.1109/PROC.1969.7278>
- Craig M, Hayashi K (2016) Surface wave surveying for near-surface site characterization in the East San Francisco Bay Area California. *Interpretation* 4(4):SQ59
- D'Amico V, Picozzi M, Baliva F, Albarello D (2008) Ambient noise measurements for preliminary site-effects characterization in the urban area of Florence, Italy. *Bull Seismological Soc Am* 98:1373–1388
- EGPC, Egyptian General Petroleum Corporation (EGPC) (1987) *Geological Map of Egypt 40 1: 500.000 – NG 36 SE GEBEL HAMATA*
- El-Hussain I, Deif A, Al-Jabri K, Mohamed AME, El-Hady S, Al-Habsi Z (2014) Efficiency of horizontal-to-vertical spectral ratio (HVSr) in defining the fundamental frequency in muscat region sultanate of oman: a comparative study. *Arab J Geosci* 7:2423–2436
- Foti S, Hollender F, Garofalo F, Albarello D, Asten M, Bard P-Y, Comina C, Cornou C, Cox B, di Giulio G, Forbriger T, Hayashi K, Lunedei E, Martin A, Mercerat D, Ohrnberger M, Poggi V, Renalier F, Sicilia D, Socco V (2018) Guidelines for the good practice of surface wave analysis: a product of the Inter PACIFIC project. *Bull Earthq Eng* 16:2367–2420. <https://doi.org/10.1007/s10518-017-0206-7>
- Gazetas G (2006) *Seismic Design of Foundations and Soil-structure Interaction*, 13th wcee – keynote address k7; 3–8 September –2006. Switzerland, Geneva
- Geopsy Software (2012) Geopsy.org packages, release 2.5.0, win32. < <https://www.geopsy.org/download.php>>
- Giegegack RF (1970) Uranium series corals from Red Sea. *Nature* 126:155–156
- Guillier B, Chatelain J-K, Bonnefoy-Claudet S, Haghshenas E (2007) Use of ambient noise: from spectral amplitude variability to H/V Stability. *J Earthquake Eng* 11:1–18
- Hamada K (1968) Ultra-micro-earthquakes in the area around Matushiro. *Bull Earthq Res Inst* 46:271–318

- Hassoup A (1987) Microearthquakes and magnitude studies on earthquake activity at Abu Dabbab region, Eastern Desert Egypt. Thesis M.Sc., Fac Sci, Cairo Univ pp 1–169
- Herrmann, RB (1994) Computer programs in seismology, vol IV, St Louis University
- Huang H-C, Tseng Y-S (2002) Characteristics of soil liquefaction using H/V of microtremors in Yuan-Lin area, Taiwan. *Terrestrial Atmospheric Oceanic Sci* 13(3):325–338
- Idriss IM (1990) Response of soft soil sites during earthquakes. H.B. Seed Memorial Symposium. Duncan JM (ed), BiTech Publishers, Vancouver, pp 273–289
- Jakosky JJ (1940) 1940. Trija publishing company, Los Angeles, California, Exploration geophysics
- Kagawa, T (1996) Estimation of Velocity Structures beneath Mexico City using Microtremor Array data. Proceeding of the 11th World Conference on Earthquake Engineering. Acapulco, Mexico
- Kebeasy RM (1990) Seismicity. In: Said R (ed) *Geology of Egypt*. Balkema, Rotterdam, pp 51–59
- KGS (2006) SurfSeis [computer software], Ver, p. 4.0 - <https://www.kgs.ku.edu/software/surfseis/>
- Khalil SM, McClay K (2002) Extensional fault related folding, north-western Red Sea. *Egypt J Struc Geol* 24:743–762
- Kim G, Hwang S (2024) Shear Wave Velocity Determination of a Complex Field Site Using Improved Nondestructive SASW Testing. *Sensors* 24(10):3231. <https://doi.org/10.3390/s24103231>
- Klemperer SL (1987) Seismic noise-reduction techniques for use with vertical stacking: An empirical comparison. *Geophysics* 52:322–334
- Koller MG, Chatelain JL, Guillier B, Duval AM, Atakan K, Lacave C, Bard PY, SESAME participants (2004) Practical user guideline and software for the implementation of the H/V ratio technique on ambient vibrations: measuring conditions, processing method and results interpretation. 13th World Conf. Earthquake Engineering (Vancouver, BC, Canada, 1–6 Aug.) Paper No. 3132
- Konno K, Ohmachi T (1998) Ground-motion characteristics estimated from spectral ratio between horizontal and vertical components of microtremor. *Bull Seismol Soc Am* 88:228–241. <https://doi.org/10.1785/BSSA0880010228>
- Kramer SL (1996) *Geotechnical Earthquake Engineering*. Prentice Hall, Englewood Cliffs
- Li P, Bo JS, Li XB, Xiao RJ (2016) Amplification effect of soil sites on ground motion in Anning River valley and Qionghai Lake area. *Chin J Geotech Eng* 38(02):362–369. <https://doi.org/10.11779/CJGE201602022>
- Ling SQ (1994) Research on the estimation of phase velocities of surface waves in microtremors, PhD thesis. Hokkaido University, Japan
- Luo Y, Xia J, Liu J, Xu Y, Liu Q (2009) Research on the middle-of-receiver-spread assumption of the MASW method. *Soil Dyn Earthq Eng* 29:71–79. <https://doi.org/10.1016/j.soildyn.2008.01.009>
- Mahajan AK, Galiana-Merino JJ, Lindholm C, Arora BR, Mundepi AK, Nitesh R, Neetu C (2011) Characterization of the sedimentary cover at the Himalayan foothills using active and passive seismic techniques. *J Appl Geophys* 2011(73):196–206
- Martínez-Soto F, Ávila F, Puertas E, Gallego R (2021) Spectral analysis of surface waves for non-destructive evaluation of historic masonry buildings. *J Cult Herit* 2021(52):31–37
- Matsushima S, Hirokawa T, De Martin F, Kawase H, Sanchez-Sesma FJ, (2014) The effect of lateral heterogeneity on horizontal-to-vertical spectral ratio of microtremors inferred from observation and synthetics. *Bull Seismol Soc Am* 104(1):381–393. <https://doi.org/10.1785/0120120321>
- Meneisy AM, Hamed A, Khalifa M, El-Bohoty M, Ghamry E, Taha A (2023) Geotechnical Zonation and Vs30 classification of soil for seismic site effects evaluation in the western extension of New Aswan City. *Egypt Pure Appl Geophys* 180:3813–3833. <https://doi.org/10.1007/s00024-023-03370-3>
- Mitchell NC, Augustin N (2017) Halokinetics and other features of GLORIA long-range sidescan sonar data from the Red Sea. *Mar Petrol Geol* 88:724–738
- Mohammed MA, Abudeif AM, Abd El-aal AK (2020) Engineering geotechnical evaluation of soil for foundation purposes using shallow seismic refraction and MASW in 15th Mayo. *Egypt J Afr Earth Sci* 162:103721
- Molnar S, Cassidy JF, Castellaro S, Cornou C, Crow H, Hunter JA, Matsushima S, Sanchez-Sesma FJ, Yong A (2018) Application of microtremor horizontal-to-vertical spectral ratio (MHVSR) analysis for site characterization: state of the art. *Surv Geophys* 39:613–631
- Mucciarelli M, Herak M, Cassidy JF (2009) Increasing seismic safety by combining engineering technologies and seismological data. Springer, Dordrecht
- Mundepi AK, Kamal (2006) thickness Effective soft sediment in Dehra Dun city, (India) using ground ambient vibration. *Himalayan Geol* 27(2):183–188
- Nakamura Y (1989) A method for dynamic characteristics estimation of sub surface using microtremor on the surface. *Railway Technical Research Institute Report* 30:25–33
- Nakamura, Y (1996) Real-time information systems for hazards mitigation. Proceedings of the 11th World Conference on Earthquake Engineering. Acapulco, Mexico, 1996
- Nakamura, Y (2000a) Clear identification of fundamental idea of Nakamura's technique and its applications. Proceedings of the 12th World Conference on Earthquake Engineering. Auckland, New Zealand
- Nakamura, Y (2000b) Clear Identification of Fundamental Idea of Nakamura 'S, *Spectrum*, p. 2656, 2000
- Nakamura, Y (2008) On the H/V spectrum, 14th World Conf. Earthq. Eng., pp. 1–10, 2008, [Online]. Available: http://117.120.50.114/papers/14wcee/14wcee_hv.pdf
- Nath RR, Kumar G, Sharma ML et al (2018) Estimation of bedrock depth for a part of Garhwal Himalayas using two different geophysical techniques. *Geosci Lett* 5:9. <https://doi.org/10.1186/s40562-018-0108-9>
- Ohuri M, Nobata A, Wakamatsu K (2002) A comparison of ESAC and FK methods of estimating phase velocity using arbitrarily shaped microtremor arrays. *Bull Seismol Soc Am* 92:2323–2332
- Okada H (2006) Theory of efficient array observations of microtremors with special reference to the SPAC method [J]. *Explor Geophys* 37(1):73–85
- Okada, H, Suto, K (2003) *The microtremor survey method*, vol. 12. Tulsa, OK: Society of Exploration Geophysicists with the cooperation of Society of Exploration Geophysicists of Japan [and] Australian Society of Exploration Geophysicists. <https://doi.org/10.1190/1.9781560801740>
- Pamuk E (2019) Investigation of the local site effects in the northern part of the eastern Anatolian region. *Turkey Boll Geofis Teor Appl* 60(4):549–568
- Park CB, Miller RD, Xia J (1999) Multichannel analysis of surface waves. *Geophysics* 64(3):800–808. <https://doi.org/10.1190/1.1444590>
- Park, CB, Carnevale, M (2010) Optimum MASW survey - Revisit after a decade of use. In: Fratta, D.O., Puppala, A.J., Muhunthan, B. (Eds.), *GeoFlorida 2010: Advances in Analysis, Modeling and Design*, pp. 1303–1312. [https://doi.org/10.1061/41095\(365\)130](https://doi.org/10.1061/41095(365)130)
- Park CS, Marx GD, Moon YS, Wiesenborn D, Chang KC, Hofman VL (1997) Alternative uses of sunflower. In: Schneiter, A.A. (Ed.), *Sunflower Technology and Production*. Agronomy Monograph no. 35. ASA, CSSA, SSSA, Madison, Wisconsin, pp. 765–807. <https://doi.org/10.2134/agronmonogr35.c17>
- Park CB, Xia J, Miller RD (1998) Imaging dispersion curves of surface waves on multi-channel record: 68th Ann Internat Mtg, Soc Expl Geophys, Expanded Abstracts, pp. 1377–1380
- Park CB, Miller RD, Xia J (2001) Offset and Resolution of Dispersion Curve in Multichannel Analysis of Surface Waves (MASW);

- Society of Exploration Geophysicists: Houston, TX, USA, 2001; p. SSM4
- Picozzi M, Parolai S, Albarello D (2005) Statistical analysis of noise horizontal to vertical spectral ratios (HVSr). *Bull Seismol Soc Am* 95 <https://doi.org/10.1785/0120040152>
- Rehman F, El-Hady SM, Atef AH, Harbi HM (2016) Multichannel analysis of surface waves (MASW) for seismic site characterization using 2D genetic algorithm at Bahrah area, Wadi Fatima Saudi Arabia. *Arab J Geosci* 9(8):1–13
- Rohmah, S, Adi Susilo, A, Yudianto, D, Hisyam, F, Eko Andi Suryo, E A, Sarjiyana (2023) Analysis of Seismic Vulnerability Index Based on Microtremor Investigation (Case Study of Majangtengah Village, Dampit, Malang Regency) 2022, AER 221, pp. 149–158, 2023. https://doi.org/10.2991/978-94-6463-148-7_16
- Salas-Romero S, Malehmir A, Snowball I, Brodic B (2021) Geotechnical site characterization using multichannel analysis of surface waves: A case study of an area prone to quick-clay landslides in southwest Sweden. *Near Surface Geophysics* 19(6):699–715. <https://doi.org/10.1002/nsg.12173>
- Sambridge M (1999) Geophysical inversion with a neighbourhood algorithm: I. Searching a parameter space. *Geophys J Int* 138:479–494
- Sambridge M (1999) Geophysical inversion with a neighbourhood algorithm: II appraising the ensemble. *Geophys J Int* 138(727–746):1999b
- Samuel, MD, Saleeb-Roufaiel, GS (1977) Lithostratigraphy and petrographic analysis of the Neogene sediments at Abu Ghusun, Um Mahara area, Red Sea coast, Egypt. In: *Beitr. Zur Lithologie, Freiburg Forsch* 323©, pp. 47–56
- Schuster GT (1998) Basics of Exploration Seismology and Tomography. Basics of Traveltime Tomography, Stanford Mathematical Geophysics Summer School Lectures
- SESAME (2004) Site effects assessment using ambient excitations European research project. <http://sesamefp5.obs.ujf-grenoble.fr>
- Shapiro, NM, Campillo, M (2004) Emergence of broadband Rayleigh waves from correlations of the ambient seismic noise. *Geophys Res Lett* 31. <https://doi.org/10.1029/2004gl019491>
- Sheehan JR, Doll WE, Mandell WA (2005) An Evaluation of Methods and Available Software for Seismic Refraction Tomography Analysis. *J Environ Eng Geophys* 10:21–34
- Steeple DW (2005) Shallow seismic methods, in: *Hydrogeophysics*, Rubin Y, Hubbard SS (eds) the Netherlands, Springer, pp 215–251. https://doi.org/10.1007/1-4020-3102-5_8
- Stipe T (2015) A Hydrogeophysical Investigation of Logan, MT Using Electrical Techniques and Seismic Refraction Tomography, Degree of Master of Science in Geoscience: Geophysical Engineering Option, Montana Tech., 179
- Taipodia, Jumrik, Dey, Arinada (2012) A Review of Active and Passive MASW Techniques: EGCEG. CBRI, Roorkee
- Telford WM, Sheriff RF (1984) “Applied Geophysics,” Cambridge University
- Toni M (2007) Geotechnical and site effect studies in Hurghada city, Red Sea, Egypt. M.Sc. thesis. Faculty of Science, Assiut University, Egypt
- Trupti S, Srinivas KNSSS, Pavan Kishore P, Seshunarayana T (2012) Site characterization studies along coastal Andhra Pradesh—India using multichannel analysis of surface waves. *J Appl Geophys* 79:82–89. <https://doi.org/10.1016/j.jappgeo.2011.12.006>
- Valenta J, Dohnal J (2007) 3D seismic travel time surveying – a comparison of the time-term method and tomography (an example from an archaeological site). *J Appl Geophys* 63:46–58
- Volant P, Cotton F, Gariel JC (1998) Estimation of site response using the H/V technique applicability and limits on Garner Valley down-hole array dataset (California). *Proceeding of 11th European Conference on Earthquake Engineering (Paris, 6–11 Sep.)* ed Bisch, Labbe and Pecker (Balkema)
- Warnana DD, Soemitro RAA, Utama W (2011) Application of microtremor HVSr method for assessing site effect in residual soil slope. *Int J Basic Appl Sci* 11(4):73–78
- Wathelet M (2005) Array recordings of ambient vibrations: surface-wave inversion. PhD thesis. Université de Liège, Belgium
- Wathelet M, Jongmans D, Ohrnberger M (2004) Surface-wave inversion using a direct search algorithm and its application to ambient vibration measurements. *Near Surface Geophysics* 2(4):211–221
- Wathelet M, Guillier B, Cornou C, Roux P, Ohrnberger M (2018) Rayleigh wave three-component beam forming: Signed ellipticity assessment from high-resolution frequency-wavenumber processing of ambient vibration arrays. *Geophys J Int* 215(1):507–523
- Xia J, Miller RD, Park CB (1999) Estimation of near-surface shear-wave velocity by inversion of Rayleigh waves. *Geophysics* 64:691–700
- Xia J, Miller RD, Park CB, Hunter JA, Harris JB, Ivanov J (2002) Comparing shear-wave velocity profiles inverted from multichannel surface wave with borehole measurements. *Soil Dyn Earthq Eng* 22(181–190):2002. [https://doi.org/10.1016/s02677261\(02\)00008-8](https://doi.org/10.1016/s02677261(02)00008-8)
- Xu P, Ling S, Li C et al (2012) Mapping deeply-buried geothermal faults using microtremor array analysis[J]. *Geophys J Int* 188(1):115–122
- Xu PF, Ling SQ, Ran WY, Liu QX, Liu JG (2013) Estimating Cenozoic thickness in the Beijing plain area using array microtremor data. *Seismol Res Lett* 84:1039–1047
- Zhang J, Toksoz M (1998) Nonlinear refraction traveltime tomography. *Geophysics* 63:1726–1737
- Zhu X, McMechan GA (1989) Estimation of two-dimensional seismic compressional wave velocity distribution by interactive tomographic imaging. *Internat J Image System Technol* 1:13–17

Publisher's Note Springer Nature remains neutral with regard to jurisdictional claims in published maps and institutional affiliations.

Springer Nature or its licensor (e.g. a society or other partner) holds exclusive rights to this article under a publishing agreement with the author(s) or other rightsholder(s); author self-archiving of the accepted manuscript version of this article is solely governed by the terms of such publishing agreement and applicable law.